Contents lists available at ScienceDirect

Applied Clay Science

journal homepage: http://ees.elsevier.com

Research paper

Effect of sepiolite treatments on the oxidation of sepiolite/natural rubber nanocomposites prepared by latex compounding technique

E. Carignani [a,b], E. Cobani [c], F. Martini [a,b], F. Nardelli [a,b], S. Borsacchi [b,*], L. Calucci [b], B. Di Credico [c,*], L. Tadiello [d], L. Giannini [d], M. Geppi [a,b,**]

[a] Department of Chemistry and Industrial Chemistry, University of Pisa, via G. Moruzzi 13, 56124 Pisa, Italy
[b] Institute for the Chemistry of the OrganoMetallic Compounds, Italian National Research Council (ICCOM-CNR), via G. Moruzzi 1, 56124 Pisa, Italy
[c] Department of Materials Science, University of Milano-Bicocca, INSTM, via R. Cozzi 55, 20125 Milano, Italy
[d] Pirelli Tyre SpA, Viale Sarca 222, 20126 Milano, Italy

ARTICLE INFO

Keywords
Clay mineral
Natural rubber
Oxidation
Latex compounding technique
MAS NMR
Relaxation times

ABSTRACT

Latex compounding technique is an economic and ecosustainable alternative to melt mixing for preparing nanocomposites in which fillers are directly mixed with natural rubber in the latex aqueous dispersion. Clay minerals are excellent potential fillers to be used in masterbatches prepared exploiting this technique, but their presence is associated to the occurrence of oxidative degradation phenomena of natural rubber. In this work, by exploiting a combination of high- and low-resolution ^{13}C and ^{1}H Solid State Nuclear Magnetic Resonance techniques, with the support of Fourier Transform Infrared spectroscopy and thermal analyses, we characterized for the first time the oxidation phenomena occurring in sepiolite/natural rubber masterbatches obtained by the latex compounding technique. Oxidized species were identified and quantified and the dynamic properties, molecular weight and thermal stability of the rubber were characterized. Moreover, the dependence of degradation phenomena on the filler treatment and on the masterbatch work-up procedure was assessed, identifying freeze-drying as the method able to effectively protect the rubber from oxidation.

1. Introduction

Natural rubber latex (NRL), a milky colloid containing poly(1,4-*cis*-isoprene), water, and minor amounts of carbohydrates, proteins, polypeptides, fatty acids, and phospholipids (Sakdapipanich and Rojruthai, 2013), can be used to easily prepare rubber nanocomposites (i.e. masterbatches, MBs) through the latex compounding technique (LCT), an economic and ecosustainable alternative to the well-established melt mixing technique (Lightsey et al., 1998). In LCT, fillers are directly mixed with rubber in the latex aqueous dispersion, without the use of silane coupling agents or additional organic molecules, commonly employed for enhancing filler-rubber interaction and filler dispersion in the polymer matrix. Indeed, the excellent dispersion properties of water allow expensive modification procedures of hydrophilic fillers to be avoided. This renders LCT particularly suited for the preparation of MBs from NRL and fillers like clay minerals, which, due to their poor compatibility with organic matrices (Bandyopadhyay et al., 2006), cannot be efficiently dispersed by melt mixing (Tan et al., 2012). Clay minerals (e.g. talc, mica, montmorillonite) are naturally occurring and readily available nanosystems that, thanks to their anisotropic structure, are regarded as very promising reinforcing fillers for polymers. In particular, sepiolite (Sep) is a natural nontoxic Mg phyllosilicate with unit cell formula $Si_{12}O_{30}Mg_8(OH)_4(H_2O)_4{\bullet}8H_2O$ available in large quantities and at low cost (Wilson, 2007). Sep is a 1D clay mineral that occurs as fibers of 0.5–10 μm length, constituted by rods with tunnel-like cavities, strictly bonded together in bundles. Therefore, its use as filler in polymer matrices usually requires chemical modifications for obtaining a uniform dispersion and consequently improving the interfacial interactions (Di Credico et al., 2018a, 2018b; Cobani et al., 2019). Sep has been extensively used as filler to improve thermal, mechanical and barrier properties of several polymers (Bokobza et al., 2009; Scotti et al., 2014; Tadiello et al., 2015). However, only few studies are reported in the literature concerning the preparation of clay mineral/natural rubber (NR) MBs by LCT (Varghese and Karger-Kocsis, 2003; Ruamcharoen et al., 2012; Varamesh et al., 2013; Othman et al., 2017). Recently an effective LCT procedure was reported to produce high-loaded Sep/NR MBs, in which

* Corresponding author.
** Corresponding author at: Department of Chemistry and Industrial Chemistry, University of Pisa, via G. Moruzzi 13, 56124 Pisa, Italy.
E-mail addresses: silvia.borsacchi@pi.iccom.cnr.it (S. Borsacchi); barbara.dicredico@unimib.it (B. Di Credico); marco.geppi@unipi.it (M. Geppi)

https://doi.org/10.1016/j.clay.2020.105528
Received 15 October 2019; Received in revised form 13 January 2020; Accepted 20 Febraury 2020
Available online xxx
0169-1317/

Sep formed a homogeneous dispersion in the rubber matrix, with inorganic domain sizes of the order of 100 nm (Di Credico et al., 2019).

Although these materials are very interesting in the research for eco-sustainable composites production, until now the application of clay mineral MBs was limited because of the poor resistance of rubber to ageing in the presence of clay mineral particles. Previous research proved that the experimental conditions applied for the MB preparation can promote oxidation and degradation of rubber, leading to a significant deterioration of its properties. This is probably due to the metal ions originally present in NRL or carried into latex by clay minerals, which could promote oxidation and thermo-degradation of the rubber matrix (Chen et al., 2001, 2006). In particular, metals with variable valence state, such as copper, manganese, and iron, are known to accelerate oxidative degradation of polymers (Scott, 1969; Chen et al., 2001, 2006). In addition, clay minerals have microporous to mesoporous structures that provide a large surface area for gas adsorption, especially for dissolved oxygen, which could be an active reagent in the degradation processes. Moreover, working in latex, water can play an active role by favoring the diffusion of oxidizing species. At last, the work-up procedure can obviously be crucial for the stability of NR in MBs.

With this in mind, in the present work we carried out a detailed characterization of different Sep/NR MBs prepared by LCT. In particular, MBs prepared with differently treated Sep and subjected to various work-up procedures were thoroughly investigated exploiting a combination of Solid State Nuclear Magnetic Resonance (SSNMR) experiments, with the support of thermal and Fourier Transform Infrared Spectroscopy (FTIR) characterizations. SSNMR is a very powerful technique for obtaining detailed structural and dynamic information on wide spatial and time scales, even in complex and/or completely amorphous materials, which can be directly analyzed without any pretreatment or dissolution (Geppi et al., 2008a, 2008b,; Borsacchi et al., 2011; Martini et al., 2011). In spite of this, only few works in the literature exploited this technique for characterizing oxidation/degradation processes of NR (Somers et al., 2000; Kehlet et al., 2014), and, in particular, no data were reported on Sep/NR nanocomposites obtained by LCT. Here high- and low-resolution ^{1}H and ^{13}C experiments were carried out on MBs prepared with either pristine Sep (SepS9) or Sep organically modified with *N*-C14–18-alkyl-*N,N*-dimethyl-benzylammonium (SepB5). Moreover, two other MBs were prepared and characterized with the aim of inspecting the effect of a controlled acid modification of SepS9 or SepB5 surface, previously applied to partially remove Mg ions, increase the amount of silanols, and decrease the Sep fiber size, thus enhancing the interfacial interactions with the polymer by silane coupling agents (Giannini et al., 2018). As far as the work-up procedure is concerned, the effects of under-vacuum heating and freeze-drying (FD) were analyzed and compared.

2. Experimental

2.1. Materials

Sep Pangel S9 (SepS9), extracted from the landfill of Vallecas (Spain), and Sep Pangel B5 (SepB5, organically-modified with *N*-C14–18-alkyl-*N,N*-dimethyl-benzylammonium) were supplied by Tolsa. NRL Medium Ammonia (MA) (60% *w*/w) was supplied by Von Bundit. HCl (37% w/w), NH_4OH (28–30% w/w), and isopropanol were purchased from Sigma-Aldrich and used without any further purification. MilliQ water with a resistivity 18.2 MΩ cm was utilized. NR was obtained by drying NRL in a vacuum oven at 80 °C for 18 h.

2.2. Preparation of SepX_33 by acid treatment

SepX_33 (X = S9 or B5) samples were prepared according to a previously reported procedure (Giannini et al., 2018). 100 g of pristine SepX were dispersed in 1.5 L of deionized water and stirred at 70 °C (600 revolution per minute (rpm)). With an automatic pH-meter, 31 mL of aqueous 37% HCl were added over a period of 7 h, at 70 °C, maintaining the pH around 3.0 ± 0.1. SepX_33 fibers were collected by centrifugation and the powders were washed several times with water and aqueous ammonium hydroxide (60%) in order to remove chloride anions, until pH 7 ± 0.2. Finally the obtained solid was dried in an oven at 100 °C for 48 h.

From the X-ray fluorescence (XRF) analysis of SepX_33 samples, 33% by weight of magnesium resulted extracted (Giannini et al., 2018).

2.3. Preparation of Sep/NR MBs

10 g of SepX or SepX_33 were dispersed in water (500 mL), sonicated for 30 min and then mixed with a mechanic stirrer (Velp Scientifica Stirrer DLS) at 500 rpm. In another vessel, 16.7 g of NRL-MA (corresponding to 10 g of dried NR) were diluted with 125 mL of distilled water and stirred for 10 min at 100 rpm. Then, the diluted NRL solution was slowly poured into the previous Sep dispersion, under stirring at 500 rpm until the flocculation of the Sep/NR MBs was completed (30 s). Sep/NR MBs were separated from the liquid phase through filtration, washed with water to remove ammonium residuals, and portioned in small pieces.

All MB samples were dried in a vacuum oven at 80 °C for 18 h (SepX/NR and SepX_33/NR). The MB prepared with SepB5_33 was also either freeze-dried by cooling down for 24 h at −14 °C and drying in a vacuum at 10^{-2} bar at room temperature for 48 h (FD-SepB5_33/NR) or dried under nitrogen at 80 °C for 48 h (N_2-SepB5_33/NR).

2.4. Characterization methods

SSNMR spectra were recorded on a Varian InfinityPlus spectrometer working at a Larmor frequency of 400.34 and 100.67 MHz for ^{1}H and ^{13}C, respectively, using a Cross Polarization-Magic Angle Spinning (CP-MAS) probehead for rotors with outer diameter of 3.2 mm. ^{1}H—^{13}C CP-MAS spectra were recorded with contact times varying between 0.1 and 7 ms, under High-Power Decoupling from ^{1}H nuclei, at a MAS frequency of 4 or 5 kHz, depending on the sample. 2000 and 4000 transients were accumulated for NR and MBs, respectively, with a recycle delay of 3 s between consecutive transients. ^{13}C Delayed CP-MAS spectra were recorded with a delay of 100 μs between the ^{1}H excitation pulse and the contact pulse, a contact time of 7 ms and accumulating 4000 transients. ^{13}C quantitative Direct Excitation (DE)-MAS spectra were recorded using the DEPTH pulse sequence for probehead background suppression (Cudby et al., 1985), under High-Power Decoupling from ^{1}H nuclei, at a MAS frequency of 6 kHz, with a recycle delay of 400 s between consecutive transients and accumulating about 800 scans. ^{1}H-MAS spectra were recorded at a MAS frequency of 4 or 5 kHz, depending on the sample, with a recycle delay of 3 s and accumulating 128 transients. ^{13}C chemical shifts were referred to hexamethylbenzene. ^{1}H Time Domain SSNMR measurements were performed at a Larmor frequency of 20.8 MHz using a Niumag permanent magnet interfaced with a Stelar PC-NMR console. A 5 mm probe was used with a ^{1}H 90° pulse duration of 3.3 μs, and a recycle delay of 0.2 s was used for all the samples. On-resonance Free Induction Decays (FIDs) were recorded for all samples using the Magic Sandwich Echo (MSE) pulse

sequence (Rhim et al., 1971; Matsui, 1991) with a total echo duration of 72 μs, using a dwell time of 1 μs, and 64 transients were accumulated. The Carr-Purcell-Meiboom-Gill (CPMG) pulse sequence (Meiboom and Gill, 1958) was used to acquire the slowly decaying component of the magnetization. The time between successive 180° pulses was 50 μs, the total number of 180° pulses was 2000 and 400 transients were accumulated for all samples.

X-ray fluorescence (XRF) spectroscopy investigations were performed using a Bruker AXS S4 Pioneer spectrometer operating at room temperature in order to quantify the amount of magnesium in the SepX_33 powders and the main metals in Sep fibers.

Electron spin resonance (ESR) studies of SepX samples were carried out at room temperature using a Bruker EMX spectrometer operating in X-Band frequency.

Attenuated total reflectance (ATR) FTIR measurements were carried out using a Perkin Elmer Spectrum 100 instrument (4 cm^{-1} resolution, 650–4000 cm^{-1} range, 16 scans).

Pristine NR and NR in MBs systems were analyzed by Gel Permeation Chromatography (GPC) using a WATER 1515 isocratic HPLC Pump, a WATER 2414 refractive index detector, and four Styragel columns (HR2, HR3, HR4, HR5). Samples were dissolved in tetrahydrofuran and the inorganic part was separated by filtration using a polytetrafluoroethylene membrane with 0.2 μm pore diameter and their chromatograms recorded with a flow of 1.0 mL/min at 35 °C. A calibration with polystyrene standards (Sigma-Aldrich) was used.

Thermogravimetric analysis (TGA) and differential scanning calorimetry (DSC) were performed with a Mettler Toledo TGA/DSC1 Star-e System under nitrogen. The variation of mass was analyzed by heating from 0 to 1000 °C, at 10 °C/min, under nitrogen flux of 50 mL/min. For DSC experiments samples were sealed into aluminum pans and heated from 30 to 350 °C at 10 °C/min. Indium was used as standard for temperature and heat flow calibration.

3. Results and discussion

3.1. Structural characterization

In order to obtain a first chemical characterization of all the different MBs, ^{13}C CP-MAS spectra were recorded and compared with that of NR (Fig. 1). In the spectrum of NR the expected signals are observed at 24.0, 27.7, 33.0, 125.6 and 135.6 ppm, which are straightforwardly ascribed to carbon nuclei of poly(1,4-*cis*-isoprene), the main NR constituent. This spectrum dramatically changes passing to the MB containing NR and pristine SepS9 (SepS9/NR). It is noteworthy that, on the whole, the spectrum of SepS9/NR closely resembles the few ^{13}C MAS NMR spectra reported in the literature for NR samples subjected to degradative oxidation arising from natural ageing or chemical attack at elevated temperatures (Somers et al., 2000; Kehlet et al., 2014).

In particular, new broad signals are evident in the spectral region typical of carbon nuclei connected with a single bond to oxygen. The weak peak centered at 64 ppm can be ascribed to epoxides, that at 74 ppm to secondary alcohols and ethers, while the signal centered at 84 ppm is indicative of peroxides and hydroperoxides (Golub et al., 1975; Aganov and Antonovskii, 1982; Rodrigues and De Paoli, 1985; Muizebelt et al., 1998; Somers et al., 2000; Kehlet et al., 2014). Also the aliphatic region (between 10 and 50 ppm) appears strongly modified, with a broadening of the NR signals and the appearance of additional broad signals underneath, compatible with the presence of aliphatic groups bonded to NR oxidized groups (Muizebelt et al., 1998; Xu et al., 2017). A clear broadening also affects NR signals at 125.6 and 135.6 ppm. These results are compatible with the main radical reactions reported for the oxidation of NR (Golub et al., 1975; Pecsok et al., 1976; Thuong et al., 2016). According to the generally accepted mechanisms, autoxidation of

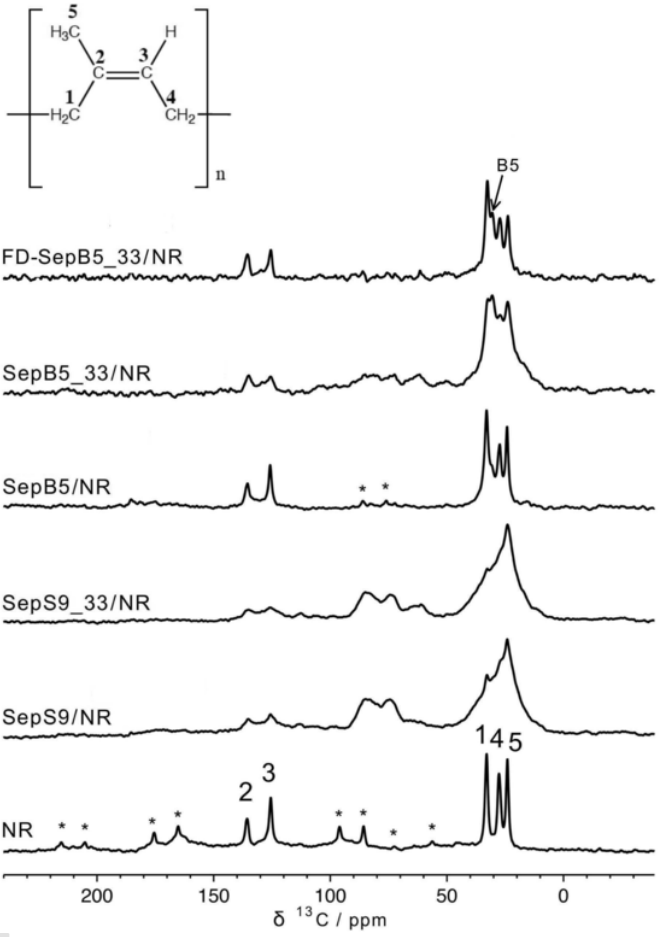

Fig. 1. ^{13}C CP-MAS spectra of NR and MB samples, recorded at a MAS frequency of 4 kHz (NR) and 5 kHz (MB samples) and with a contact time of 2 ms. Numbers indicate peak assignment to carbon nuclei of the NR repeating unit, as reported in the figure. Asterisks indicate spinning sidebands. The arrow with B5 label indicates the signal of the organic cation of SepB5.

poly(1,4-*cis*-isoprene) occurs through free-radical chain reactions in which hydroperoxides (ROOH) are the primary products, the decomposition of which is responsible for the reaction being autocatalytic. The peroxy radical ROO• is generated in the initiation stage by the decomposition of ROOH and/or in the propagation stage by the addition of an oxygen molecule to a polyisoprenyl radical R• (allylic radicals), in turn formed by extraction of an α-methylenic hydrogen from an isoprenic unit. Peroxy radicals can undergo intramolecular addition to double bonds in adjacent isoprenic units, ultimately leading to the incorporation of epoxides in the polymer chain and formation of alkoxy radicals RO•, which may either abstract hydrogen to form alcohols or undergo scission. The formed radicals can attack isoprenic units of the same or other polymeric chains giving cross-linking or undergo chain scission with production of ketones or aldehydes. Bimolecular reactions involving RO• and/or R• radicals represent the termination stage, which can result in cross-linking (Golub et al., 1975; Pecsok et al., 1976).

The ^{13}C CP-MAS spectrum of SepS9/NR clearly indicates that NR oxidation processes occur in the presence of SepS9 when a vacuum-oven work-up is used. This can be ascribed to several concomitant reasons: i) the entrapping of oxygen in the Sep porous structure and the presence of residual oxygen in the oven, ii) the presence of metal ions catalyzing the oxidative reactions and iii) the presence of residual water molecules embedded in the Sep structure, favoring the diffusion of the oxidizing species. In particular, transition metal ions

are known to catalyze the autoxidation of polyisoprenoids (Farley et al., 1993) by increasing the rate of decomposition of hydroperoxides, and, indeed, metals present as impurities in clay minerals have been found to promote degradative oxidation of MBs prepared with NRL (Chen et al., 2001, 2006). In our case, metals present in Sep samples were characterized by means of XRF analysis. In addition to magnesium being the main structural ion of SepX crystalline structure, Al, K, Ti, Fe, Ca, Mn, Cu and Zn elements were detected in small amounts, as shown in Table S1. In particular, Fe ions, present at low but not negligible percentage in all samples (about 0.6 wt%) and being mainly present as Fe^{3+} (see ESR spectra in Fig. S1), could be considered as possible catalysts for the detected oxidation processes. Concerning this, Cornejo et al. (Cornejo et al., 1983) studied the role of both adsorbed and structural Fe^{3+} in natural Sep fibers with respect to the oxidation reaction in aqueous dispersion, demonstrating its significant catalytic activity.

On the other hand, it must also be mentioned that a spectrum similar to that of SepS9/NR was recently reported also for hybrids of silica and epoxidized natural rubber (ENR), in which a grafting of ENR to silica surface was hypothesized, through the opening reaction of the epoxy group with Si-OH. In particular, the signals of the formed Si-O-C and –COH groups were identified at 86.1 ppm and 75.2 ppm (Xu et al., 2017). Considering the abundance of Si-OH groups in Sep, this reaction could also be relevant for our MBs (Hayeemasae and Ismail, 2019).

All the spectral features described for SepS9/NR can be observed also in the spectrum of the MB prepared with the acid treated Sep and subjected to the same heating in vacuum oven (SepS9_33/NR). In this case, the peak centered at 64 ppm is more intense, suggesting an increment of epoxide groups, and all the NR signals are further broadened.

On the other hand, in the ^{13}C CP-MAS spectrum of the MB prepared with the organically modified SepB5 (SepB5/NR), the appearance of the NR signals is substantially the same as in pristine NR (Fig. 1). In addition, in this spectrum the resonances at 31 and 33 ppm of the methylene carbons of the organic cation of SepB5 (indicated by an arrow and the label B5 in Fig. 1), partly overlapping with NR signals, can be recognized. These two signals indicate that the aliphatic chains of the cation are present in both *all-trans* and disordered *trans-gauche* conformations (Kitamaru et al., 1986), as also observed in the ^{13}C CP-MAS spectrum of pristine SepB5 (see Fig. S2). Since the work-up procedure is the same used for the MBs with SepS9 and SepS9_33 and the metal contents of the different Sep samples are very similar (Table S1), the different oxidation behavior can be ascribed to a different accessibility of radicals to metal centers. In particular, the organic cation molecules inside the Sep pores and covering the Sep surface can partially "protect" the Sep fibers and thus prevent the diffusion of both oxygen and metal ions during MB preparation, as similarly reported in the literature (Chen et al., 2001, 2006).

If the MB is prepared with SepB5_33, that is SepB5 previously modified by acid treatment, the "protective" effect is reduced because of a partial removal of the organic cation (about 55% according to TGA analysis). The ^{13}C CP-MAS spectrum of SepB5_33/NR shows clear signs of oxidative degradation, even if less pronounced than in the spectra of SepS9/NR and SepS9_33/NR.

Conversely, the ^{13}C CP-MAS spectrum of FD-SepB5_33/NR (Fig. 1) clearly indicates that when heating in vacuum-oven is replaced by freeze-drying the oxidation of NR is substantially prevented.

The ^{13}C NMR results are corroborated by ATR-FTIR analysis, which was carried out on all samples. In particular, the FTIR spectra of SepS9/NR, SepB5_33/NR and FD-SepB5_33/NR are here discussed in comparison with that of pristine NR. In Fig. 2, the light grey shadow areas highlight the most significant changes in the infrared bands of MB samples.

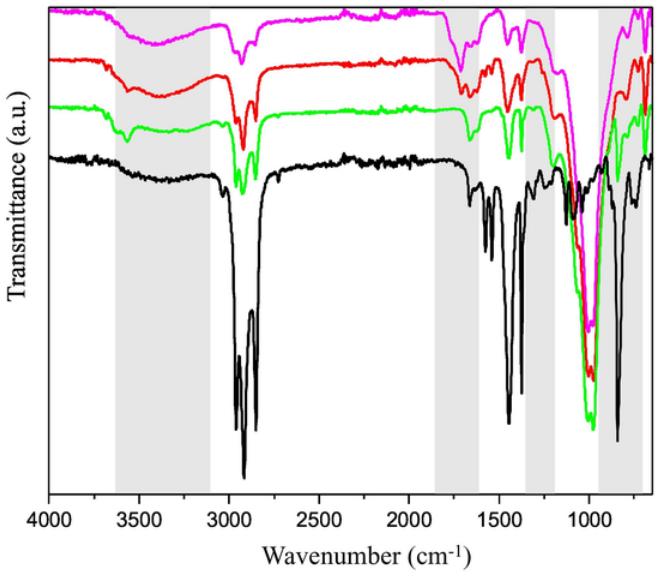

Fig. 2. FTIR spectra of NR (black line), SepS9/NR (violet line), SepB5_33/NR (red line), and FD- SepB5_33/NR (green line). The light grey shadow areas highlight the most significant spectral regions. (For interpretation of the references to colour in this figure legend, the reader is referred to the web version of this article.)

The spectrum of NR (black line in Fig. 2) shows the characteristic bands of poly(1,4-*cis*-isoprene), in line with already reported data (Lu and Hsu, 1987), while in the MBs spectra it is possible to identify also the bands of Sep fillers. In detail, the spectrum of SepS9/NR (violet line) presents a significant broad band in the region between 3200 and 3600 cm^{-1}, also existing in the spectrum of SepB5_33/NR (red line). The appearance of this band, absent in the NR spectrum, may be due to the formation of hydroxyl groups (–OH) as a result of the NR oxidation. In the 3400–3700 cm^{-1} spectral region adsorption bands ascribable to the OH stretching vibrations of Mg-OH groups and water molecules in Sep fibers are also present (Casal et al., 2001).

The FTIR spectral regions related to the polyisoprene backbone chain are analyzed more in depth in Fig. 3. First, for SepS9/NR and SepB5_33/NR it is possible to observe the presence of bands at 1650–1800 cm^{-1} (Fig. 3a), associable to the formation of ketone or aldehyde and ester, acid and amide, not observed in the ^{13}C CP-MAS NMR spectra probably due to their low amount and their scarce cross-polarization efficiency. In addition, the intensity of the bands at about 1310 cm^{-1} (Fig. 3b), related to methylene groups in the NR backbone, and at 840 cm^{-1} (Fig. 3c), assigned to *cis*-methine groups, decreases significantly for the MBs worked-up in vacuum-oven. This corresponds to changes in the degree of substitution of the carbon atoms of the *cis*-1,4 double bonds in the polyisoprene chain.

These observations support the occurrence of oxidation reactions in the MBs obtained with vacuum-oven work-up. On the other hand, FTIR spectra confirm that the FD work-up preserves the NR from oxidation. This points to a major role of heating and presence of water/oxygen in promoting radical reactions, factors which are both avoided in FD. It is worth mentioning that oxidation phenomena were also prevented when the work up procedure consisted in heating under nitrogen, a procedure that guarantees a more effective removal of residual oxygen. Indeed, all the characterization techniques indicated that N_2-SepB5_33/NR is equivalent to FD-SepB5_33/NR (see for instance the ^{13}C CP-MAS spectrum of N_2-SepB5_33/NR shown in Fig. S3).

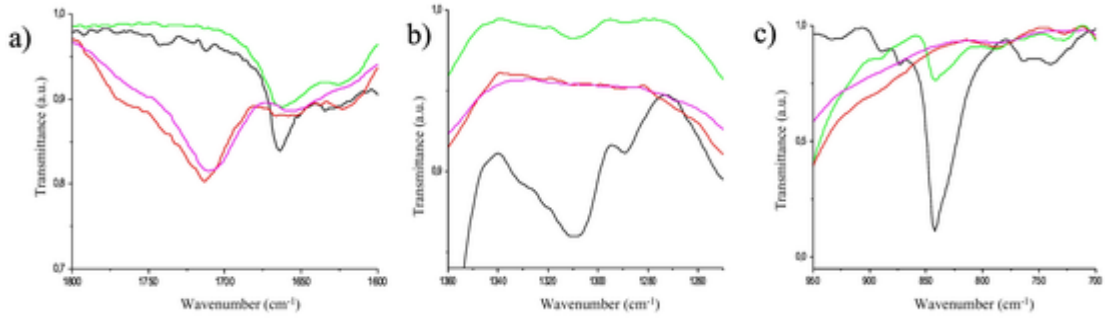

Fig. 3. Expansion of the FTIR spectra of NR (black line), SepS9/NR (violet line), SepB5_33/NR (red line), and FD-SepB5_33/NR (green line) in the ranges: (a) 1600–1800 cm^{-1}, (b) 1250–1400 cm^{-1} and 700–950 cm^{-1}. (For interpretation of the references to colour in this figure legend, the reader is referred to the web version of this article.)

With the aim of quantifying the extent of oxidation in the MBs dried in oven, we recorded ^{13}C DE-MAS spectra with a long recycle delay between consecutive scans, which ensures complete magnetization recovery for all carbon nuclei. In fact, the ^{13}C MAS spectra previously discussed (Fig. 1) were recorded by exploiting CP from ^{1}H to ^{13}C nuclei, which, occurring through ^{1}H—^{13}C dipolar couplings, intrinsically favors the signals of ^{13}C nuclei spatially close to ^{1}H and belonging to rigid moieties (molecular mobility averages out dipolar interactions, thus reducing the efficiency of CP). If for solid samples CP usually increases sensitivity, on the other hand signal intensities cannot be considered quantitative. The quantitative ^{13}C DE-MAS spectra of SepS9_33/NR and SepB5_33/NR are reported in Fig. 4. In both spectra, it is possible to recognize the already identified broad signals of oxidized NR, superimposed to the narrow peaks of the non-oxidized polymer and SepB5 cation (in the case of SepB5_33/NR). An estimate of the extent of NR oxidation could be obtained from the ratio between the sum of the areas of the narrow NR signals (obtained by spectral fitting) and the whole spectral area. It was found that non-oxidized NR is responsible of about 20% and 30% of the whole spectral area in the case of SepS9_33/NR and SepB5_33/NR MBs, respectively.

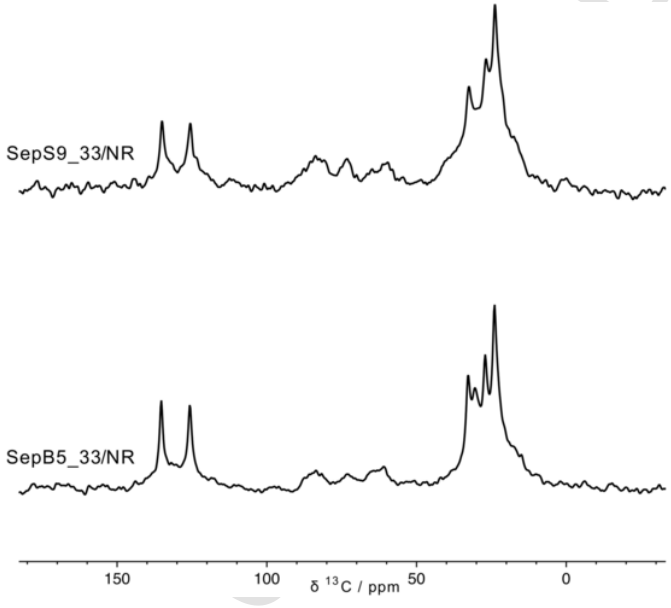

Fig. 4. Quantitative ^{13}C DE-MAS spectra of (bottom) SepB5_33/NR and (top) SepS9_33/NR MBs.

3.2. Dynamics characterization

From the comparison between DE-MAS and CP-MAS spectra, it is evident that CP favors the broad signals associated to oxidized NR. This indicates that the oxidized polymer moieties are quite rigid, as it is expected for the introduction of polar groups, since this might bring on one side to a polymer with increased Tg and on the other side to the formation of stronger interactions between the oxidized polymer moieties and the filler particles. This was further confirmed by ^{13}C Delayed CP-MAS experiments, which suppress signals of carbon nuclei in very rigid environments (i.e. dipolar coupled with ^{1}H nuclei with a very short transverse relaxation time T_2). In the case of the most degraded SepS9_33/NR MB, no signals could be detected, while for SepB5_33/NR MB only residual non-oxidized NR signals were observed (Fig. S4).

A deeper characterization of the dynamic properties of the different samples could be obtained from the measurement and analysis of ^{1}H transverse relaxation times (T_2). In Fig. 5, the first part of the ^{1}H FIDs of NR and MBs samples, recorded with the MSE pulse sequence in on-resonance conditions at low magnetic field, is shown.

The reproduction of the ^{1}H FID of a sample with a linear combination of analytical functions ($f_i(t)$), each characterized by a weight percentage (w_i) and a T_2 value (T_2^i), is an established method for recognizing domains of hydrogen nuclei characterized by different mobility (Eq. 1).

$$F(t) = \frac{\sum_i w_i f_i(t)}{100} \quad (1)$$

T_2 monotonically increases with mobility and the weight of each function is proportional to the number of ^{1}H nuclei in the corresponding domain. Through a fitting procedure it was possible to obtain a good reproduction of the ^{1}H FIDs of all samples with a combination of a Gaussian ($f_{Gau}(t) = \exp(-(t/T_2^{Gau})^2)$) and a Weibullian ($f_{Weib}(t) = exp(-(t/T_2^{Weib})^a)$) function, the former with $T_2^{Gau} \approx 19$–25 μs and the latter with $T_2^{Weib} \geq 400$ μs (and $a = 1.00$–1.55). This roughly indicates that in all samples ^{1}H nuclei are distributed in two kinds of motionally distinct domains: one with very restricted mobility, the other much more mobile. The weights of these two components, reported in Table 1, vary quite much from one MB to the other.

On the basis of the ^{1}H FID analysis of the pristine components (among which only that of NR is here reported), it can be considered that ^{1}H nuclei belonging to SepX and SepX_33 mainly contribute to the short T_2 component, while protons of NR are mainly characterized by a long T_2. The results obtained for SepB5/NR and FD-SepB5_33/NR are very similar to those expected on the basis of samples composition, under the hypothesis that the dynamic properties of the single components do not substantially change in passing from pris-

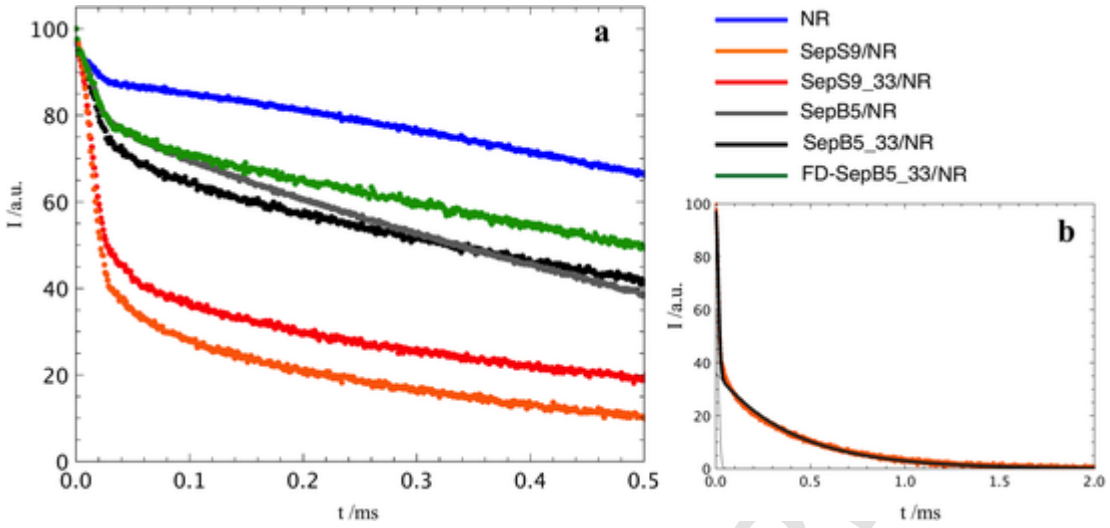

Fig. 5. (a) Expansion of the first 0.5 ms of the on-resonance ^{1}H FIDs of the indicated samples, recorded with the MSE pulse sequence; (b) fit of the experimental FID of SepS9/NR to a linear combination of a Gaussian (T_2^{Gau} = 19 μs) and a Weibullian (T_2^{Weib} = 400 μs) function.

Table 1
Weight percentages of the Gaussian (w_{Gau}, %) and Weibullian (w_{Weib}, %) functions in the linear combination of functions best fitting the experimental FIDs of the indicated samples, recorded with the MSE pulse sequence. Values of 1/*PWRA* calculated from the T_2 values measured for the different samples by the CPMG experiment. Estimated maximum errors are reported in the column headers.

Sample	w_{Gau} (±2%)	w_{Weib} (±2%)	1/*PWRA* (±0.01 ms)
NR	9%	91%	5.87 ms
SepS9/NR	62%	38%	2.16 ms
SepS9_33/NR	55%	45%	2.08 ms
SepB5/NR	19%	81%	4.51 ms
SepB5_33/NR	26%	74%	3.47 ms
FD-SepB5_33/NR	22%	78%	5.04 ms

tine components to MBs. This is reasonable also considering that in these samples NR does not undergo significant degradation. On the other hand, the results obtained for SepS9/NR and SepS9_33/NR highlight a substantial stiffening of the samples, which can be related to the observed oxidation. It can be noted that in the case of SepB5_33/NR the increase of the very rigid fraction is less dramatic, in agreement with what already observed in ^{13}C Delayed CP-MAS spectra.

With the aim of comparing the dynamic characteristics of the mobile fraction of all samples, ascribable to non-oxidized NR, the corresponding ^{1}H T_2's were better determined from CPMG experiments. Considering that the signal decay of the mobile fraction of each sample resulted to be well described by a combination of two exponential functions, each characterized by a value of T_2, we calculated the Population Weighted Rate Average (*PWRA*), defined as:

$$PWRA = 10^{-2} \sum_i \frac{w_i}{T_2^i} \quad (2)$$

being T_2^i the *i*-th T_2 component, with weight percentage w_i. *PWRA* is representative of the overall mobility and its inverse can be considered as a sort of average T_2, which in general increases with the degree of mobility. The 1/*PWRA* values of the different samples reported in Table 1 clearly indicate that NR experiences only a slight stiffening in the less or not degraded MBs (i.e. SepB5/NR and FD-SepB5_33/NR). On the contrary, a remarkable reduction of mobility is observed for SepB5_33/NR and becomes very strong in the MBs prepared with SepS9 and SepS9_33. These results are further confirmed by ^{1}H-MAS spectra (Fig. 6), in which, especially at the low MAS frequency here used, only signals of ^{1}H nuclei in mobile environments can be resolved. For all samples, the only observed signals are those of NR, more intense for the non-oxidized samples, less for SepB5_33/NR and strongly depressed for both SepS9/NR and SepS9_33/NR. No additional signals ascribable to oxidized groups could ever be resolved, confirming their very scarce mobility.

3.3. GPC and thermal characterization

Taking into account that the molecular weight of NR is of great importance for the properties and processability of rubber materials, GPC analysis was performed (Fig. S5) in order to determine the change of the poly(cis-1,4-isoprene) molecular weight in MB samples; results are shown in Table 2.

The GPC profile of pristine NR is bimodal, exhibiting two peaks of the weight-average molecular weight (Mw), as already reported. The major peak exists at a Mw of about $2.35 \cdot 10^5$ g/mol, in line with reported values for commercially used rubbers ranging from 10^4 to 10^6 g/mol (Kovuttikulrangsie and Sakdapipanich, 2005). A minor peak is also present, due to the biosynthesis metabolism process in the phospholipid chain end of molecules, which affects the extent of Mw on rubber molecules.

With respect to NR, GPC analyses of SepX_33/NR MBs reveal a significant shift in the Mw to lower values, especially for SepS9_33/NR ($0.03 \cdot 10^5$ g/mol). On the other hand, this shift is moderate for SepB5/NR and even less pronounced for FD-SepB5_33/NR. These results clearly confirm that in the MBs subjected to vacuum-oven work-up oxidation produced degradation of the carbon backbone of poly(cis-1,4-isoprene), while only very little degradation took place for the MB obtained by FD (green line in Fig. S5).

Polydispersity or molecular weight distribution values were estimated by dividing Mw by the number-average molecular weight (Mn). It is commonly accepted that a ratio of 1.0 refers to a sample containing molecules of one size, while higher ratios indicate a significant distribution in the rubber molecules size (Wood and Cornish, 2000). For our samples, polydispersity values show that MBs prepared with modified SepX_33 are strongly affected by the oxidation process. The polydispersity value ranges from about 2.4 to 3.6, suggesting the presence of a molecular weight distribution or a mixture of small and large rubber molecules (Table 2). Instead the SepB5/NR sample has a polydispersity value closer to that of pristine

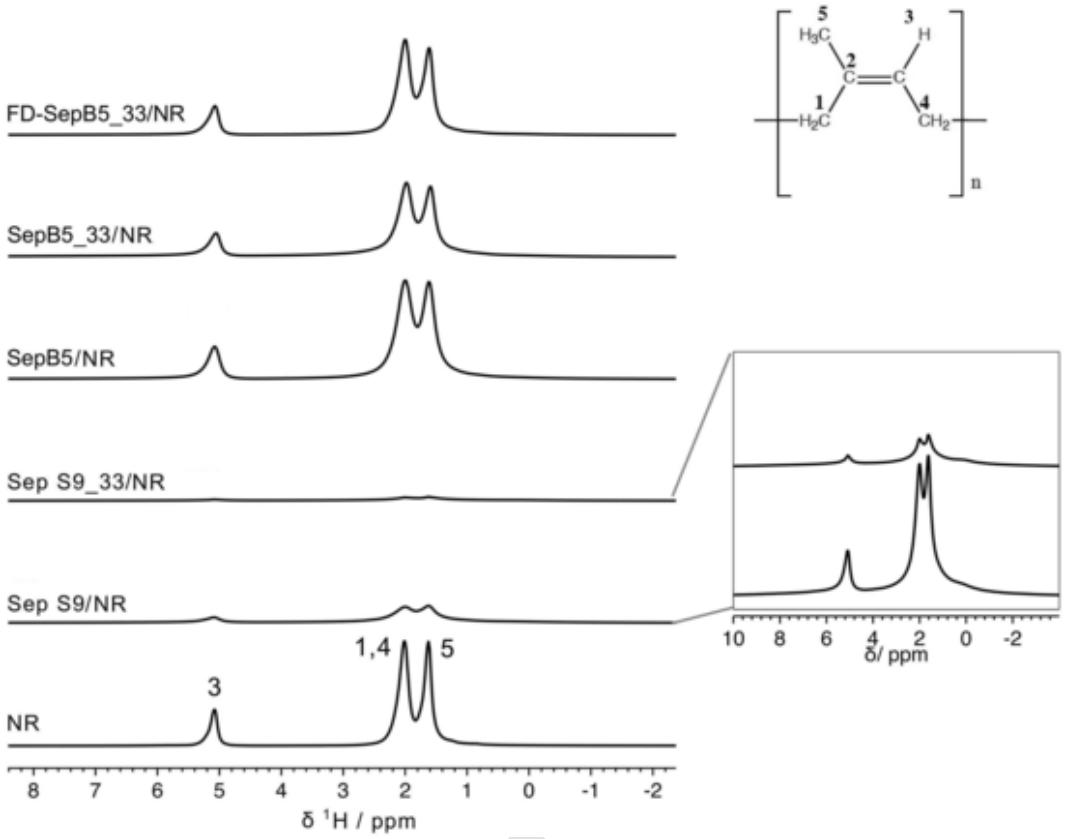

Fig. 6. ^{1}H-MAS spectra of NR and MB samples, recorded at a MAS frequency of 4 kHz (NR) and 5 kHz (MB samples). All spectra are reported on the same intensity scale. In the inset, the spectra of SepS9/NR and SepS9_33/NR MBs are shown on a ten times enhanced intensity scale. Numbers indicate the peak assignment to hydrogen nuclei of the NR repeating unit, as reported in the figure.

Table 2
Number-average molecular weight (Mn), weight-average molecular weight (Mw), higher average molecular weight (Mz), and polydispersity index = Mw/Mn of NR and MB samples.

	Mn (g/mol)	Mw (g/mol)	Mz (g/mol)	Polydispersity
NR	$2.13 \cdot 10^5$	$2.35 \cdot 10^5$	$2.55 \cdot 10^5$	1.10
SepS9_33/NR	$0.01 \cdot 10^5$	$0.03 \cdot 10^5$	$0.06 \cdot 10^5$	2.36
SepB5/NR	$0.52 \cdot 10^5$	$1.03 \cdot 10^5$	$1.57 \cdot 10^5$	1.99
SepB5_33/NR	$0.07 \cdot 10^5$	$0.26 \cdot 10^5$	$0.67 \cdot 10^5$	3.57
FD-SepB5_33/NR	$1.17 \cdot 10^5$	$1.57 \cdot 10^5$	$1.93 \cdot 10^5$	1.34

NR, suggesting a slight effect of the oxidation process. Above all, the sample obtained by FD shows a polydispersity index very similar to that of NR, in line with the above reported results.

In addition, the thermal stability of the different samples was investigated by TGA/DSC thermal analysis, which can be an indicator of the ability of materials to maintain the required properties at a desired temperature. The thermal degradation of NR and MBs was investigated under inert atmosphere. The TGA and DSC curves of NR, SepS9_33/NR, SepB5_33/NR, and FD-SepB5_33/NR MBs are reported in Fig. 7 as representative samples. As expected, NR (black dotted line) is thermally stable until 250 °C. At higher temperatures, thermal decomposition of NR starts, probably producing monomers, dimers, trimers, etc.

Compared to NR, the decomposition of SepB5_33/NR (red dotted line) starts much earlier at 150 °C, while for SepS9_33/NR (blue dotted line) a mass loss is already observed at 50 °C. Considering that a signal due to adsorbed water was not observed in the ^{1}H-MAS NMR

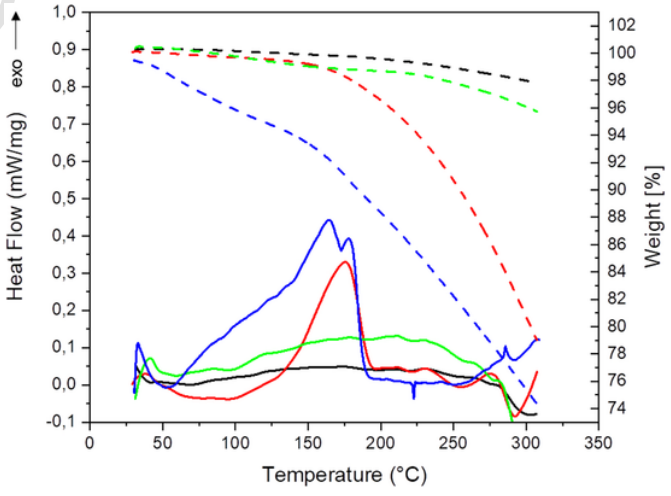

Fig. 7. TGA (dotted lines) and DSC (solid lines) curves of NR (black), SepS9_33/NR (blue), SepB5_33/NR (red), FD-SepB5_33/NR (green). (For interpretation of the references to colour in this figure legend, the reader is referred to the web version of this article.)

spectrum of SepS9_33/NR, such mass loss must be ascribed to rubber degradation. On the other hand, the FD-SepB5_33/NR sample (green dotted line) starts to degrade at 250 °C, with a thermal decay similar to that of NR. This confirms that the FD procedure provides MB samples with higher thermal stability with respect to samples thermally dried under vacuum.

Degradation phenomena were investigated more in depth by DSC, which can highlight the endothermic or exothermic processes

happening in the MBs materials, giving information on the reactions that occur at a specific temperature. DSC thermograms (Fig. 7) of bare NR (black line) and FD-SepB5_33/NR (green line) display a flat baseline, suggesting that the materials remain stable until 250 °C, in line with TGA curves. Instead, the DSC profiles of SepS9_33/NR (blue line) and SepB5_33/NR (red line) show an excursion in the exothermic direction in the 50–200 °C and 130–200 °C ranges, respectively, suggesting that these materials undergo significant degradation at lower temperature with respect to NR.

4. Conclusions

The application of a multi-nuclear and multi-technique SSNMR approach, including high and low-resolution ^{13}C and ^{1}H experiments, also supported by FTIR, GPC and thermal analyses, to a set of MBs based on NR and different kinds of Sep, obtained by LCT and subjected to different work-up procedures, allowed detailed information on the oxidative degradation affecting NR to be obtained. The results clearly indicate that, when the work-up consists in heating in a vacuum-oven MBs prepared with pristine or acid treated Sep, NR undergoes oxidative degradation ascribable to the action of residual oxygen, metal ions and possibly water present in the Sep pore structure. The oxidation mainly results in the formation of epoxy, hydroxyl, ether, peroxy and hydroperoxy groups, associated to a noticeable stiffening of the oxidized polymer moieties. On the other hand, oxidation can be inhibited when Sep fibers are suitably modified with an organic cation, as in the case of SepB5, which probably protects the rubber matrix from the oxidizing species during the MB preparation. Moreover, it was demonstrated that when FD or heating under nitrogen are used as work-up procedures oxidation does not occur even if the MB is prepared with the acid treated SepB5_33, suggesting a major role of water and residual oxygen in promoting radical oxidative reactions. This is the first time that products of degradative oxidation of NR in MBs with sepiolites are clearly identified and their structural and dynamic properties are characterized in detail.

Funding

This work was supported by Regione Toscana and Pirelli Tyre SpA (POR FSE 2014-2020 Asse A - "NMR4DES" project).

Declaration of Competing Interest

None.

Acknowledgments

Dr. Irene Tagliaro (University of Milano-Bicocca) is acknowledged for performing some FTIR and TGA measurements. Authors thank Prof. Roberto Scotti (University of Milano-Bicocca) for giving conceptual advices.

Appendix A. Supplementary data

Supplementary data to this article can be found online at https://doi.org/10.1016/j.clay.2020.105528.

References

Aganov, A.V., Antonovskii, V.L., 1982. 13C NMR spectra of organic peroxides. Bull. Acad. Sci. USSR Div. Chem. Sci. 31, 247–250. doi:10.1007/BF00948235.

Bandyopadhyay, A., Maiti, M., Bhowmick, A.K., 2006. Synthesis, characterisation and properties of clay and silica based rubber nanocomposites. Mater. Sci. Technol. 22, 818–828. doi:10.1179/174328406X101265.

Bokobza, L., Leroy, E., Lalanne, V., 2009. Effect of filling mixtures of sepiolite and a surface modified fumed silica on the mechanical and swelling behavior of a styrene-butadiene rubber. Eur. Polym. J. 45, 996–1001. doi:10.1016/j.eurpolymj.2008.12.028.

Borsacchi, S., Martini, F., Geppi, M., Pilati, F., Toselli, M., 2011. Structure, dynamics and interactions of complex sol–gel hybrid materials through SSNMR and DSC: Part II, ternary systems based on PE–PEG block copolymer, PHS and silica. Polymer 52, 4545–4552. doi:10.1016/J.POLYMER.2011.07.055.

Casal, B., Merino, J., Serratosa, J.M., Ruiz-Hitzky, E., 2001. Sepiolite-based materials for the photo- and thermal-stabilization of pesticides. Appl. Clay Sci. 18, 245–254. doi:10.1016/S0169-1317(01)00030-8.

Chen, M., Ao, N.J., Chen, Y., Yu, H.P., Qian, H.L., Wang, C., Zhou, H.L., Qu, J.L., Guo, C.K., 2001. Study on aging of clay-rubber masterbatch from modified clay. J. Appl. Polym. Sci. 82, 338–342. doi:10.1002/app.1857.

Chen, M., Ao, N.J., Liao, Y.Y., Chen, Y., Zhou, H.L., 2006. Thermo-oxidative degradation of natural rubber/clay composite. J. Appl. Polym. Sci. 100, 3809–3815. doi:10.1002/app.23808.

Cobani, E., Tagliaro, I., Geppi, M., Giannini, L., Leclère, P., Martini, F., Nguyen, T.C., Lazzaroni, R., Scotti, R., Tadiello, L., Di Credico, B., 2019. Hybrid interface in sepiolite rubber nanocomposites: role of self-assembled nanostructure in controlling dissipative phenomena. Nanomaterials 9, 1–19. doi:10.3390/nano9040486.

Cornejo, J., Hermosin, M.C., White, J.L., Barnes, J.R., Hem, S.L., 1983. Role of ferric iron in the oxidation of hydrocortisone by sepiolite and palygorskite. Clay Clay Miner. 31, 109–112. doi:10.1346/CCMN.1983.0310204.

Cudby, M.E.A., Harris, R.K., Metcalfe, K., Packer, K.J., Smith, P.W.R., Bunn, A., 1985. ^{13}C and ^{1}H n.m.r. studies of solid polyolefines. Polymer 26, 169–176. doi:10.1016/0032-3861(85)90026-6.

Di Credico, B., Cobani, E., Callone, E., Conzatti, L., Cristofori, D., D'Arienzo, M., Dirè, S., Giannini, L., Hanel, T., Scotti, R., Stagnaro, P., Tadiello, L., Morazzoni, F., 2018. Size-controlled self-assembly of anisotropic sepiolite fibers in rubber nanocomposites. Appl. Clay Sci. 152, 51–64. doi:10.1016/j.clay.2017.10.032.

Di Credico, B., Redaelli, M., Bellardita, M., Calamante, M., Cepek, C., Cobani, E., D'Arienzo, M., Evangelisti, C., Marelli, M., Moret, M., Palmisano, L., Scotti, R., 2018. Step-by-step growth of HKUST-1 on functionalized TiO_2 surface: an efficient material for CO_2 capture and solar photoreduction. Catalysts 8, 353. doi:10.3390/catal8090353.

Di Credico, B., Tagliaro, I., Cobani, E., Conzatti, L., D'Arienzo, M., Giannini, L., Mascotto, S., Scotti, R., Stagnaro, P., Tadiello, L., 2019. A green approach for preparing high-loaded sepiolite/polymer biocomposites. Nanomaterials 9, 46. doi:10.3390/nano9010046.

Farley, P.S., Porter, M., Banthorpe, D.V., 1993. Effect of adventitious iron on epoxidation of natural rubber latex. J. Nat. Rubb. Res. 7, 157–167.

Geppi, M., Borsacchi, S., Mollica, G., 2008. Solid-state NMR of organic/inorganic multicomponent materials. In: Encyclopedia of Magnetic Resonance. John Wiley & Sons, Ltd, Chichester, UK. doi:10.1002/9780470034590.emrstm1014.

Geppi, M., Borsacchi, S., Mollica, G., Veracini, C.A., 2008. Applications of Solid-state NMR to the study of organic/inorganic multicomponent materials. Appl. Spectrosc. Rev. 44, 1–89. doi:10.1080/05704920802352564.

Giannini, L., Tadiello, L., Hanel, T., Cobani, E., Di Credico, B., D'Arienzo, M., Scotti, R., Morazzoni, F., Perez Chacho, J.J., Julve, S., Daniel, J., 2018. PCT Int. Appl. WO 2018078500 A1 20180503.

Golub, M.A., Hsu, M.S., Wilson, L.A., 1975. Nuclear magnetic resonance study of thermal oxidationof polyisoprene. Rubber Chem. Technol. 48, 953–971. doi:10.5254/1.3539699.

Hayeemasae, N., Ismail, H., 2019. Reinforcement of epoxidized natural rubber through the addition of sepiolite. Polym. Compos. 40, 924–931. doi:10.1002/pc.24762.

Kehlet, C., Catalano, A., Dittmer, J., 2014. Degradation of natural rubber in works of art studied by unilateral NMR and high field NMR spectroscopy. Polym. Degrad. Stab. 107, 270–276. doi:10.1016/j.polymdegradstab. 2013.12.039.

Kitamaru, R., Horii, F., Murayama, K., 1986. Phase structure of lamellar crystalline polyethylene by solid-state high-resolution ^{13}C NMR: detection of the crystalline-amorphous interphase. Macromolecules 19, 636–643. doi:10.1021/ma00157a026.

Kovuttikulrangsie, S., Sakdapipanich, J.T., 2005. The molecular weight (MW) and molecular weight distribution (MWD) of NR from different age and clone Hevea trees. J. Sci. Technol. 27, 337–342.

Lightsey, J.W., Kneiling, D.J., Long, J.M., 1998. Silica wet masterbatch: a new process for pre-dispersion of silica in emulsion polymers. Rubber World 218, 35–40.

Lu, F.J., Hsu, S.L., 1987. A Vibrational spectroscopic analysis of the structure of natural rubber. Rubber Chem. Technol. 1987 (60), 647–658.

Martini, F., Borsacchi, S., Geppi, M., Pilati, F., Toselli, M., 2011. Structure, dynamics and interactions of complex sol–gel hybrid materials through SSNMR and DSC: part I, binary systems based on PE-PEG block copolymer, PHS and silica. Polymer 52, 4536–4544. doi:10.1016/J.POLYMER.2011.07.054.

Matsui, S., 1991. Solid-state NMR imaging by magic sandwich echoes. Chem. Phys. Lett. 179, 187–190. doi:10.1016/0009-2614(91)90313-X.

Meiboom, S., Gill, D., 1958. Modified spin-echo method for measuring nuclear relaxation times. Rev. Sci. Instrum. 29, 688–691. doi:10.1063/1.1716296.

Muizebelt, W.J., Donkerbroek, J.J., Nielen, M.W.F., Hussem, J.B., Biemond, M.E.F., Klaasen, R.P., Zabel, K.H., 1998. Oxidative crosslinking of alkyd resins studied with mass spectrometry and NMR using model compounds. J. Coatings Technol. 70, 83–92. doi:10.1007/BF02720501.

Othman, N., Muttalib, S.N.A., Ismail, N.I., 2017. The effect of surface modification on the properties of palygorskite filled natural rubber nanocomposite. Macromol. Symp. 371, 35–43. doi:10.1002/masy.201600035.

Pecsok, R.L., Painter, P.C., Shelton, J.R., Koenig, J.L., 1976. Fourier transform infrared studies of the mechanism of oxidation of cis-1,4-polybutadiene. Rubber Chem. Technol. 49, 1010–1018. doi:10.5254/1.3534984.

Rhim, W.K., Pines, A., Waugh, J.S., 1971. Time-reversal experiments in dipolar-coupled spin systems. Phys. Rev. B 3, 684–696. doi:10.1103/PhysRevB.3.684.

Rodrigues, M.A., De Paoli, M.A., 1985. The chemical effects of photo-oxidation on isoprene rubber. Eur. Polym. J. 21, 15–23. doi:10.1016/0014-3057(85)90058-8.

Ruamcharoen, J., Chotisuwan, S., Ruamcharoen, P., 2012. Tensile properties and morphology of natural rubber-kaolinite organoclay composites. In: Advanced Materials Research. Trans Tech Publications Ltd, pp. 701–705. doi:10.4028/www.scientific.net/AMR.488-489.701.

Sakdapipanich, J.T., Rojruthai, P., 2013. Natural Rubber: Biosynthesis, Structure, Properties and Application, in: Narural Rubber Materials. 1. Royal Society of Chemistry, Cambridge, UK, pp. 28–52. doi:10.1039/9781849737647-00028.

Scott, G., 1969. Degradation and stabilization of polymers. Eur. Polym. J. 5, 189–213. doi:10.1016/S0014-3057(69)80012-1.

Scotti, R., Conzatti, L., D'Arienzo, M., Di Credico, B., Giannini, L., Hanel, T., Stagnaro, P., Susanna, A., Tadiello, L., Morazzoni, F., 2014. Shape controlled spherical (0D) and rod-like (1D) silica nanoparticles in silica/styrene butadiene rubber nanocomposites: Role of the particle morphology on the filler reinforcing effect. Polymer 55, 1497–1506. doi:10.1016/j.polymer.2014.01.025.

Somers, A.E., Bastow, T.J., Burgar, M.I., Forsyth, M., Hill, A.J., 2000. Quantifying rubber degradation using NMR. Polym. Degrad. Stab. 70, 31–37. doi:10.1016/S0141-3910(00)00076-8.

Tadiello, L., D'Arienzo, M., Di Credico, B., Hanel, T., Matejka, L., Mauri, M., Morazzoni, F., Simonutti, R., Spirkova, M., Scotti, R., 2015. The filler-rubber interface in styrene butadiene nanocomposites with anisotropic silica particles: morphology and dynamic properties. Soft Matter 11, 4022–4033. doi:10.1039/c5sm00536a.

Tan, J., Wang, X., Luo, Y., Jia, D., 2012. Rubber/clay nanocomposites by combined latex compounding and melt mixing: a masterbatch process. Mater. Des. 34, 825–831. doi:10.1016/j.matdes.2011.07.015.

Thuong, N.T., Yamamoto, Y., Nghia, P.T., Kawahara, S., 2016. Analysis of damage in commercial natural rubber through NMR spectroscopy. Polym. Degrad. Stab. 123, 155–161. doi:10.1016/j.polymdegradstab. 2015.11.025.

Varamesh, A., Abdollahi, M., Khanli, H.H., 2013. Structure and properties of NR/BR blend/clay nanocomposites prepared by the latex method. Polym. Sci. - Ser. A 55, 115–120. doi:10.1134/S0965545X13020119.

Varghese, S., Karger-Kocsis, J., 2003. Natural rubber-based nanocomposites by latex compounding with layered silicates. Polymer 44, 4921–4927. doi:10.1016/S0032-3861(03)00480-4.

Wilson, I., 2007. Applied Clay Mineralogy. Occurrences, processing and application of kaolins, bentonite, palygorskitesepiolite, and common clays. Clay Clay Miner. 55, 644–645. doi:10.1007/bf03406033.

Wood, D.F., Cornish, K., 2000. Microstructure of purified rubber particles. Int. J. Plant Sci. 161, 435–445. doi:10.1086/314269.

Xu, T., Jia, Z., Wang, S., Chen, Y., Luo, Y., Jia, D., Peng, Z., 2017. Self-crosslinkable epoxidized natural rubber–silica hybrids. J. Appl. Polym. Sci. 134, 44605. doi:10.1002/app.44605.